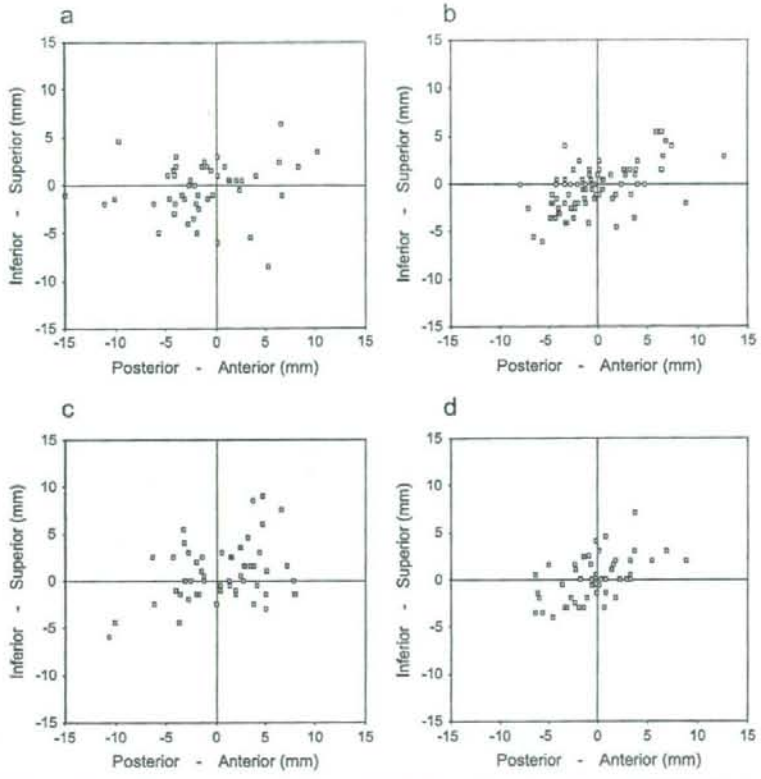

Fig. 6. Scatter plot of prostate movement in sagittal plane (superoinferior [Y] and posteroanterior [Z] directions). (a) Without gas removal in non-whole pelvic radiotherapy (WPRT) arm. (b) With gas removal in non-WPRT arm. (c) Without gas removal in WPRT arm. (d) With gas removal in WPRT arm.

the non-WPRT arm, and in the Z direction ($p = 0.005$) for the WPRT arm (Table 3). The 95% confidence limit displacements of the seminal vesicle COM (CLS) in the rectal gas removal group was smaller than in the non–gas removal group in all directions. The 95% CLS was reduced by 0.4 mm in the X direction, 0 mm in the Y direction, and 1.9 mm in the Z direction for the non-WPRT arm with rectal gas removal. For the WPRT arm, the 95% CLS was reduced by 0.7 mm in the X direction, 1 mm in the Y direction, and 4.1 mm in the Z direction. In these groups, the overall SD, maximum, and 95% CLS of the seminal vesicles were smallest in all directions for patients with rectal gas removal in the WPRT arm.

The results of the separation of the overall prostate and seminal vesicle variations in Σ and σ are given in Tables 4 and 5. Statistical significance with rectal gas removal was noted in the random deviation of the prostate in the X and Z directions in all patients and in the non-WPRT arm. Except for the σ values in the Y and Z directions in the WPRT arm, all Σ and σ values of the prostate with rectal gas removal were smaller than those with no gas removal. Statistical significance with rectal gas removal was noted only in the random deviation of the seminal vesicles in the Z direction in all patients and the non-WPRT arm, and the Σ value in the Z direction in the WPRT arm. Except for the Σ values in the Y direction for all patients and non-WPRT arm, and σ values in the Y direction for WPRT arms, all Σ and σ values of the seminal vesicles with rectal gas removal were smaller than those with no gas removal. In these groups, the Σ values of the prostate and seminal vesicles were smallest in all directions for patients with rectal gas removal in the WPRT arm. Except for the Y direction in seminal vesicles, $2.5\ \Sigma + 0.7\ \sigma$ of the prostate and seminal vesicles were smallest in all directions for patients with rectal gas removal in the WPRT arm.

DISCUSSION

A correlation between the rectal volume changes and movement of the prostate and seminal vesicles has been reported by many investigators (13–16). Several studies have reported that the prostate moves mainly in the Y and

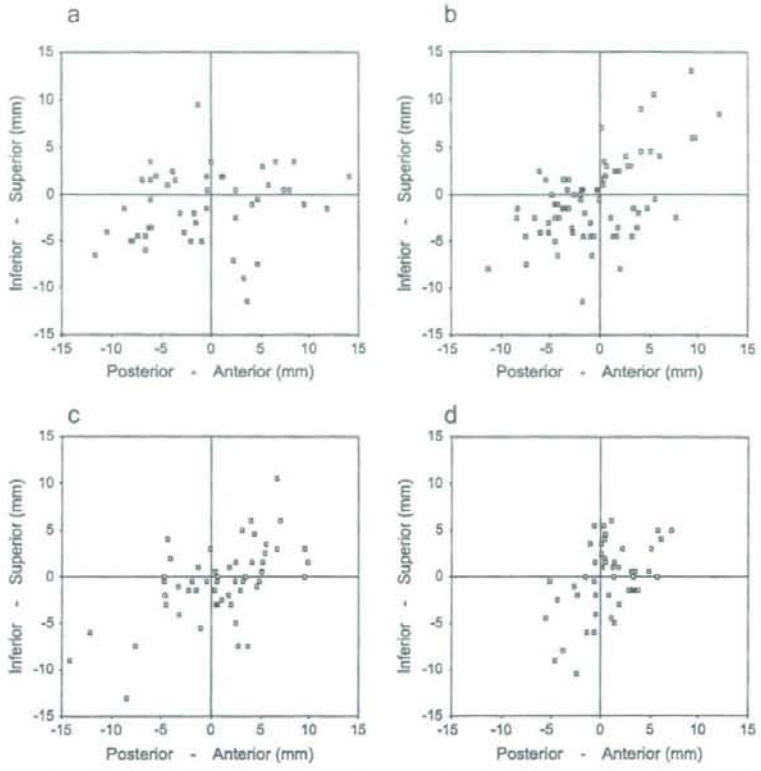

Fig. 7. Scatter plot of seminal vesicle movement in sagittal plane (inferosuperior [Y] and anteroposterior [Y] directions). (a) Without gas removal in non-whole pelvic radiotherapy (WPRT) arm (b) With gas removal in non-WPRT arm. (c) Without gas removal in WPRT arm. (d) With gas removal in WPRT arm.

Z directions and that it moves anteriorly with increasing rectal distension (13, 14, 16–21).

Although some investigators contoured the rectum starting at the anus and moving up to the position at which the rectum turns horizontally into the sigmoid colon (12, 20, 22, 23), others delineated the rectum using a length equal to the length of the clinical target volume (CTV) plus margins (9–11, 24). To decrease patient variability and compare our results with other reported results, we used the CSA to evaluate the effect of the rectum on prostate and seminal vesicle motion.

Pinkawa *et al.* (22) reported critical values of CSA >12 cm^2 that demonstrated a steep increase in the posterior margin necessary to cover the subsequent CTV positions. According to their report, a posterior margin of 1.0 cm and complete CTV coverage resulted in only 50% of subsequent CTV positions with a CSA >12 cm^2 vs. 94%with a CSA ≤12 cm^2. de Crevoisier *et al.* (12) reported that with a posterior margin of 0.75–1.0 cm, the incidence of biochemical failure was significantly greater among patients with a CSA of >11.2 cm^2 on the planning CT scan. In our results, the CSA in the rectal gas removal group was significantly smaller in all patients and in the WPRT arm. The CSA before RT was <9 cm^2 in all patients with gas removal. During RT, the CSA was <9 cm^2 for all gas removal patients in the WPRT arm.

Although the use of laxatives to minimize pelvic organ filling and motion of the prostate has been recommended (13, 25), their use was reported only before acquisition of the planning CT scan or images (9–11, 25). In contrast, some oncologists are reluctant to advise all patients to take a laxative before the acquisition of the planning CT scan (23). They advocate that the use of laxatives might empty the rectum too much and that the prostate would on average be displaced posteriorly in the preparation stage. It might also be impractical to use laxatives daily for patients with diarrhea because of WPRT. Furthermore, no clinical study has proved the beneficial effect of regularly used laxatives on reducing the rectal volume and prostate motion.

We instructed patients to evacuate the rectal gas by inserting their index finger into their anus to widen the rectal canal, followed by cleaning the rectum with a jet of water. This method did not increase rectal urgency, even in patients in

Table 2. Center of mass motion for the prostate over all fractions and all patients

	Patients (*n*)	M (mm)	SD (mm)	*p*	Minimum (mm)	Maximum (mm)	90% CLP (mm)	95% CLP (mm)
All patients								
Left–right (X)								
No gas removal	102	0.1	1.2	0.028	−2.4	3.4	1.9	2.4
Gas removal	126	0	0.9		−2	2.4	1.5	1.7
Superoinferior (Y)								
No gas removal	102	0.3	3	0.065	−8.5	9	5.0	6.0
Gas removal	126	−0.2	2.4		−6	7	3.5	4.5
Anteroposterior (Z)								
No gas removal	102	−0.3	4.7	0.016	−15	10.2	7.8	10.1
Gas removal	126	−0.3	3.7		−8	12.7	6.4	6.9
No WPRT								
Left–right (X)								
No gas removal	48	−0.1	1.1	0.183	−2.4	3.3	1.8	2.4
Gas removal	78	0	0.9		−2	2.4	1.3	1.6
Superoinferior (Y)								
No gas removal	48	−0.4	2.9	0.22	−8.5	6.5	5.0	6.0
Gas removal	78	−0.4	2.4		−6	5.5	4.0	5.5
Anteroposterior (Z)								
No gas removal	48	−1.3	4.9	0.32	−15	10.2	9.7	10.2
Gas removal	78	−0.3	4		−8	12.7	6.6	7.4
WPRT								
Left–right (X)								
No gas removal	54	0.3	1.2	0.113	−2.1	3.4	2.1	2.5
Gas removal	48	0.1	1		−1.9	2.1	1.7	1.9
Superoinferior (Y)								
No gas removal	54	0.8	3.1	0.13	−6	9	5.5	7.5
Gas removal	48	0.1	2.4		−4	7	3.5	4.0
Anteroposterior (Z)								
No gas removal	54	0.7	4.3	0.047	−10.7	8.5	7.2	8.5
Gas removal	48	−0.3	3.4		−6.4	8.9	6.2	6.4

Abbreviations: CLP = confidence limit displacements of prostate center of mass; other abbreviations as in Table 1.
p Values given for SD are results of F tests comparing deviations with and without gas removal.

the WPRT arm. All patients tolerated this procedure, and no patients refused. The vector of the prostate and seminal vesicle displacement in the rectal gas removal group was significantly smaller in all patients by ANOVA. The maximal, 90%, and 95% confidence limits of the prostate and seminal vesicle displacement vector in the rectal gas removal group were smaller than in the non–gas removal group. The 95% confidence limit of the prostate displacement vector was reduced by 2.5 mm in all patients, 2.3 mm in the non-WPRT arm, and 2.9 mm in the WPRT arm with rectal gas removal. The 95% confidence limit of the seminal vesicle displacement vector was reduced by 1.1 mm in all patients, 0.3 mm in the non-WPRT arm, and 4.4 mm in the WPRT arm with rectal gas removal. Clinical concerns exist about the perturbation of the radiation dose near the air–tissue interfaces and underdosing of targets because of the presence of an air cavity (26). Rectal gas removal can decrease both prostate motion and perturbation of the radiation dose near the prostate.

Differences in treatment techniques and organ motion measurement techniques make it very difficult to compare the results of the various published studies. Some made the measurements of organ motion from the edges of the organ structures (14, 17) and some analyzed organ motion by the COM (11, 13, 16, 20, 24). We selected the COM for organ motion measurement to be able to compare our results with those of other studies. In other studies of organ motion measured by COM, the overall SD of the prostate movements was 0.7–0.9 mm in the X, 3.2–3.9 mm in the Y, and 2.6–3.9 mm in the Z directions (11, 13, 16, 20). In contrast, the overall SD of seminal vesicle movements was 1.7–3.2 mm in the X, 3.5–5.5 mm in the Y, and 3.8–7.3 mm in the Z directions (11, 16, 20). RT was delivered to the prostate and seminal vesicles in these studies. Comparing our results with these studies, a smaller SD was noted in patients with gas removal in the WPRT arm, especially in the Y direction for prostate motion (2.4 mm) and the Z direction for seminal vesicle motion (3 mm).

The overall prostate and seminal vesicle variations have been separated into systematic and random variations. van Lin *et al.* (6) reported Σ and σ of the prostate was 0.7, 2.8, and 2.2 mm and 1.3, 1.9, and 2.5 mm in the X, Y, and Z directions, respectively. Patients were treated in the supine position and advised to use a laxative diet before CT scanning and daily RT. Similar results were reported by Zelefsky *et al.* (11). The Σ and σ of the prostate was 0.6, 2.7, and 2.4 mm and 0.5, 1.6, and 2.0 mm in the X, Y, and Z directions, respectively (11). They also reported that the Σ and σ of the seminal

Table 3. Center of mass motion for seminal vesicles for all fractions and all patients

	Patients (n)	M (mm)	SD (mm)	p	Minimum (mm)	Maximum (mm)	90% CLS (mm)	95% CLS (mm)
All patients								
Left–right (X)								
No gas removal	102	−0.3	2.3	0.035	−10	4.8	3.2	4.0
Gas removal	126	−0.2	1.9		−7.7	4.6	3.1	3.9
Superoinferior (Y)								
No gas removal	102	−0.9	4	0.534	−13	10.5	7.0	9.0
Gas removal	126	−0.3	4.2		−11.5	13	6.5	8.5
Anteroposterior (Z)								
No gas removal	102	0.1	5.5	0.002	−14.2	14	8.7	10.5
Gas removal	126	0	4.2		−11.3	12.1	6.6	8.4
No WPRT								
Left–right (X)								
No gas removal	48	−0.1	2.6	0.035	−10	4.8	3.5	4.4
Gas removal	78	−0.3	2		−7.7	4.6	3.1	4.0
Superoinferior (Y)								
No gas removal	48	−1.3	3.9	0.627	−11.5	9.5	7.0	9.0
Gas removal	78	−0.4	4.4		−11.5	13	7.5	9.0
Anteroposterior (Z)								
No gas removal	48	−0.6	6.1	0.032	−11.6	14	9.5	11.6
Gas removal	78	−0.4	4.7		−11.3	12.1	8.3	9.7
WPRT								
Left–right (X)								
No gas removal	54	−0.5	1.9	0.37	−4.6	4.1	3.1	4.1
Gas removal	48	−0.2	1.8		−3.4	4.1	3.2	3.4
Superoinferior (Y)								
No gas removal	54	−0.6	4.1	0.837	−13	10.5	7.5	9.0
Gas removal	48	−0.2	3.9		−10.5	6	6.0	8.0
Anteroposterior (Z)								
No gas removal	54	0.8	5	0.005	−14.2	9.9	8.5	9.9
Gas removal	48	0.7	3		−5.5	7.2	5.5	5.8

Abbreviations: CLS: confidence limit displacements of the seminal vesicles center of mass; other abbreviations as in Table 1.
p Values given for SD are results of F tests comparing deviations with and without gas removal.

vesicles was 2.6, 4.8, and 3.9 mm and 1.7, 2.7, and 3.0 mm in the X, Y, and Z directions, respectively. Their patients underwent CT scanning in the prone treatment position with an individually designed immobilization device. All patients were instructed to use a Fleet enema the night before and the day of the simulation procedure. A rectal catheter was inserted at the simulation procedure. Compared with these studies, our results for the gas removal group in the WPRT arm suggested a smaller Σ in the Y direction (1.8 mm) for prostate motion and all directions for seminal vesicle motion (X, 1.4 mm; Y, 3.2 mm; and Z, 2.3 mm). Except for the σ values in the Y and Z directions in the WPRT arm, all Σ and σ values of the prostate with rectal gas removal were smaller than those with no gas removal. Except for the Σ values in the Y direction for all patients and the non-WPRT arms and the σ values in the Y direction for the WPRT arm, all Σ and σ values of the seminal vesicles with rectal gas removal were smaller than those with no gas removal.

Some investigators proposed recipes for automatic calculation of the CTV-PTV margins to account for both systematic and random errors (21, 27). To ensure a minimal dose to the CTV of 95% for 90% of the patients, van Herk *et al.* (21) determined that $2.5\ \Sigma + 0.7\ \sigma$ is required for a margin between the CTV and PTV. According to their recipe, the prostate margin was reduced by 0.4 mm in the X direction, 1.2 mm in the Y direction, and 2.4 mm in the Z direction for the non-WPRT arm with rectal gas removal. For the WPRT arm, the margin of the prostate was reduced by 0.8 mm in the X direction, 2.3 mm in the Y direction, and 2.8 mm in the Z direction. For the seminal vesicles, except in the Y direction in the non-WPRT arm, the margin was reduced by 1.1 mm in the X direction and 2.6 mm in the Z direction for the non-WPRT arm by rectal gas removal. For the WPRT arm, the margin of the seminal vesicles was reduced by 0.4 mm in the X direction, 0.7 mm in the Y direction, and 5.7 mm in the Z direction. Reduction of the prostate by >2 mm was noted in the Z direction for the non-WPRT arm and WPRT arm and in the Y direction for the WPRT arm. The reduction of the seminal vesicle motion by >4 mm was noted in the Z direction for the WPRT arm. These results were similar to the 95% CLP and CLS reduction with rectal gas removal.

CONCLUSIONS

This is the first clinical study to prove the beneficial effects of rectal gas removal by patients on reducing prostate and seminal vesicle motion. With rectal gas removal, the CSA

Table 4. Center of mass motion for prostate: systemic deviations and random deviations

	Σ (mm)	*p*	σ (mm)	*p*	2.5 Σ + 0.7 σ
All patients					
Left–right (X)					
No gas removal	0.9	0.063	1	0.003	2.9
Gas removal	0.7		0.8		2.2
Superoinferior (Y)					
No gas removal	2.6	0.347	2	0.799	7.9
Gas removal	1.9		1.9		6.0
Anteroposterior (Z)					
No gas removal	4.1	0.109	2.8	0.025	12.3
Gas removal	3.1		2.5		9.6
No WPRT					
Left–right (X)					
No gas removal	0.8	0.557	1	0.018	2.6
Gas removal	0.7		0.8		2.2
Superoinferior (Y)					
No gas removal	2.3	0.833	2.1	0.64	7.3
Gas removal	2		1.8		6.1
Anteroposterior (Z)					
No gas removal	4.1	0.534	3.4	0.003	12.7
Gas removal	3.4		2.5		10.3
WPRT arm					
Left–right (X)					
No gas removal	1	0.212	0.9	0.119	3.1
Gas removal	0.7		0.8		2.3
Superoinferior (Y)					
No gas removal	2.7	0.194	1.9	0.485	8.1
Gas removal	1.8		2		5.8
Anteroposterior (Z)					
No gas removal	4	0.176	2	0.894	11.5
Gas removal	2.8		2.5		8.7

Abbreviations: Σ = systematic deviation; σ = random deviation; other abbreviations as in Table 1.

p Values given for SD are results of F tests comparing deviations with and without gas removal.

Table 5. Center of mass motion for seminal vesicles: systemic deviations and random deviations

	Σ (mm)	*p*	σ (mm)	*p*	2.5 Σ + 0.7 σ
All patients					
Left–right (X)					
No gas removal	1.7	0.552	1.9	0.233	5.5
Gas removal	1.6		1.4		4.8
Superoinferior (Y)					
No gas removal	3.3	0.385	3	0.632	10.3
Gas removal	3.4		2.9		10.4
Anteroposterior (Z)					
No gas removal	4.5	0.096	4	0.003	14.1
Gas removal	3.5		2.8		10.7
No WPRT					
Left–right (X)					
No gas removal	1.8	0.843	2.3	0.087	6.2
Gas removal	1.7		1.4		5.1
Superoinferior (Y)					
No gas removal	2.9	0.373	3.3	0.307	9.6
Gas removal	3.7		2.9		11.4
Anteroposterior (Z)					
No gas removal	4.6	0.434	5	0.003	14.9
Gas removal	4		3.1		12.3
WPRT arm					
Left–right (X)					
No gas removal	1.5	0.499	1.4	0.956	4.8
Gas removal	1.4		1.3		4.4
Superoinferior (Y)					
No gas removal	3.5	0.748	2.7	0.672	10.6
Gas removal	3.2		2.8		9.9
Anteroposterior (Z)					
No gas removal	4.5	0.049	2.9	0.298	13.2
Gas removal	2.3		2.4		7.5

Abbreviations as in Tables 1 and 4.

p Values given for SD are results of F tests comparing deviations with and without gas removal.

was decreased, resulting in reduced motion and reduced CTV-PTV margins of the prostate and seminal vesicles. In the WPRT arm, the smallest Σ values of the prostate and seminal vesicles of all groups were obtained in most directions with rectal gas removal. This is especially important for WPRT patients who require RT to the prostate, seminal vesicles, and PLNs, because either PLN or prostate gland movement cannot be corrected by image-guided RT in patients undergoing WPRT. Rectal gas evacuation using the patient's index finger and a jet of water can be performed safely without rectal urgency. We recommend this procedure, especially for patients who require WPRT.

REFERENCES

1. Lattanzi J, McNeeley S, Pinover W, *et al.* A comparison of daily CT localization to a daily ultrasound-based system in prostate cancer. *Int J Radiat Oncol Biol Phys* 1999;43:719–725.
2. Morr J, DiPetrillo T, Tsai JS, *et al.* Implementation and utility of a daily ultrasound-based localization system with intensity-modulated radiotherapy for prostate cancer. *Int J Radiat Oncol Biol Phys* 2002;53:1124–1129.
3. Smitsmans MH, de Bois J, Sonke JJ, *et al.* Automatic prostate localization on cone-beam CT scans for high precision image-guided radiotherapy. *Int J Radiat Oncol Biol Phys* 2005;63: 975–984.
4. Herman MG, Pisansky TM, Kruse JJ, *et al.* Technical aspects of daily online positioning of the prostate for three-dimensional conformal radiotherapy using an electronic portal imaging device. *Int J Radiat Oncol Biol Phys* 2003;57:1131–1140.
5. Wu J, Haycocks T, Alasti H, *et al.* Positioning errors and prostate motion during conformal prostate radiotherapy using on-line isocentre set-up verification and implanted prostate markers. *Radiother Oncol* 2001;61:127–133.
6. van Lin EN, van der Vight LP, Witjes JA, *et al.* The effect of an endorectal balloon and off-line correction on the interfraction systematic and random prostate position variations: A comparative study. *Int J Radiat Oncol Biol Phys* 2005;61:278–288.
7. Lawton CA, Desilvio M, Roach M 3rd, *et al.* An update of the phase III trial comparing whole pelvic to prostate only radiotherapy and neoadjuvant to adjuvant total androgen suppression: Updated analysis of RTOG 94-13, with emphasis on unexpected hormone/radiation interactions. *Int J Radiat Oncol Biol Phys* 2007;69:646–655.
8. Roach M 3rd, DeSilvio M, Lawton C, *et al.* Phase III trial comparing whole-pelvic versus prostate-only radiotherapy and

neoadjuvant versus adjuvant combined androgen suppression: Radiation Therapy Oncology Group 9413. *J Clin Oncol* 2003; 21:1904–1911.
9. Pickett B, Roach M 3rd, Verhey L, *et al.* The value of nonuniform margins for six-field conformal irradiation of localized prostate cancer. *Int J Radiat Oncol Biol Phys* 1995;32:211–218.
10. Stroom JC, Koper PC, Korevaar GA, *et al.* Internal organ motion in prostate cancer patients treated in prone and supine treatment position. *Radiother Oncol* 1999;51:237–248.
11. Zelefsky MJ, Crean D, Mageras GS, *et al.* Quantification and predictors of prostate position variability in 50 patients evaluated with multiple CT scans during conformal radiotherapy. *Radiother Oncol* 1999;50:225–234.
12. de Crevoisier R, Tucker SL, Dong L, *et al.* Increased risk of biochemical and local failure in patients with distended rectum on the planning CT for prostate cancer radiotherapy. *Int J Radiat Oncol Biol Phys* 2005;62:965–973.
13. Antolak JA, Rosen II, Childress CH, *et al.* Prostate target volume variations during a course of radiotherapy. *Int J Radiat Oncol Biol Phys* 1998;42:661–672.
14. Beard CJ, Kijewski P, Bussiere M, *et al.* Analysis of prostate and seminal vesicle motion: Implications for treatment planning. *Int J Radiat Oncol Biol Phys* 1996;34:451–458.
15. Crook JM, Raymond Y, Salhani D, *et al.* Prostate motion during standard radiotherapy as assessed by fiducial markers. *Radiother Oncol* 1995;37:35–42.
16. Roeske JC, Forman JD, Mesina CF, *et al.* Evaluation of changes in the size and location of the prostate, seminal vesicles, bladder, and rectum during a course of external beam radiation therapy. *Int J Radiat Oncol Biol Phys* 1995;33:1321–1329.
17. Padhani AR, Khoo VS, Suckling J, *et al.* Evaluating the effect of rectal distension and rectal movement on prostate gland position using cine MRI. *Int J Radiat Oncol Biol Phys* 1999;44: 525–533.
18. Dawson LA, Mah K, Franssen E, *et al.* Target position variability throughout prostate radiotherapy. *Int J Radiat Oncol Biol Phys* 1998;42:1155–1161.
19. Melian E, Mageras GS, Fuks Z, *et al.* Variation in prostate position quantitation and implications for three-dimensional conformal treatment planning. *Int J Radiat Oncol Biol Phys* 1997;38:73–81.
20. Tinger A, Michalski JM, Cheng A, *et al.* A critical evaluation of the planning target volume for 3-D conformal radiotherapy of prostate cancer. *Int J Radiat Oncol Biol Phys* 1998;42:213–221.
21. van Herk M, Bruce A, Kroes AP, *et al.* Quantification of organ motion during conformal radiotherapy of the prostate by three dimensional image registration. *Int J Radiat Oncol Biol Phys* 1995;33:1311–1320.
22. Pinkawa M, Siluschek J, Gagel B, *et al.* Influence of the initial rectal distension on posterior margins in primary and postoperative radiotherapy for prostate cancer. *Radiother Oncol* 2006; 81:284–290.
23. Hoogeman MS, van Herk M, de Bois J, *et al.* Strategies to reduce the systematic error due to tumor and rectum motion in radiotherapy of prostate cancer. *Radiother Oncol* 2005;74: 177–185.
24. Zellars RC, Roberson PL, Strawderman M, *et al.* Prostate position late in the course of external beam therapy: Patterns and predictors. *Int J Radiat Oncol Biol Phys* 2000;47:655–660.
25. Villeirs GM, DeMeerleer GO, Verstraete KL, *et al.* Magnetic resonance assessment of prostate localization variability in intensity-modulated radiotherapy for prostate cancer. *Int J Radiat Oncol Biol Phys* 2004;60:1611–1621.
26. Li XA, Yu C, Holmes T. A systematic evaluation of air cavity dose perturbation in megavoltage x-ray beams. *Med Phys* 2000;27:1011–1017.
27. Stroom JC, de Boer HC, Huizenga H, *et al.* Inclusion of geometrical uncertainties in radiotherapy treatment planning by means of coverage probability. *Int J Radiat Oncol Biol Phys* 1999;43: 905–919.

International Journal of Medicine and Medical Sciences Vol.1(1) pp. 001-008, January, 2009
Available online http://www.academicjournals.org/ijmms

Full Length Research Paper

Diagnostic modeling with differences in plasma amino acid profiles between non-cachectic colorectal/breast cancer patients and healthy individuals

Naoyuki Okamoto[1]*, Yohei Miyagi[2], Akihiko Chiba[3], Makoto Akaike[4], Manabu Shiozawa[4], Akira Imaizumi[5], Hiroshi Yamamoto[6], Toshihiko Ando[5], Minoru Yamakado[7] and Osamu Tochikubo[8]

[1]Cancer Prevention and Cancer Control Division, Kanagawa Cancer Center, 1-1-2, Nakao, Asahi-ku, Yokohama-city, 241-0815 Japan.
[2]Moleculer Pathology and Genetics Division, Kanagawa Cancer Center, 1-1-2, Nakao, Asahi-ku, Yokohama-city, 241-0815 Japan.
[3]Department of Breast Surgery, Kanagawa Cancer Center, 1-1-2, Nakao, Asahi-ku, Yokohama-city, 241-0815 Japan.
[4]Department of Gastrointestinal Surgery, Kanagawa Cancer Center, 1-1-2, Nakao, Asahi-ku, Yokohama-city, 241-0815 Japan.
[5]Institute of Life Sciences, Ajinomoto CO., Inc., Japan.
[6]HI Department, Ajinomoto CO., Inc. , Japan.
[7]Center for Multiphasic Health Testing and Services, Mitsui Memorial Hospital, Japan.
[8]Department of Public Health, Yokohama City University, Graduate School of Medicine, Japan.

Accepted 22 December, 2008.

Metabolic changes in patients with cancer lead to alterations in their amino-acid balances. Thus, amino-acid profiles may be useful as biomarkers of cancers. This study was conducted to analyze amino-acid profiles in plasma by multivariate analysis, in order to elucidate differences between cancer patients and controls. Venous blood samples were taken from colorectal and breast cancer patients, and healthy controls. Plasma free amino acids were measured by liquid chromatography/mass spectrometry. No weight loss was observed in any of the cancer patients. Multiple logistic regression models were used to discriminate between cancer patients and controls. The area under the curve (AUC) of the receiver operating characteristic (ROC) curve for each discriminant score was calculated as 0.860 (95% confidence interval: 0.784 to 0.937) for colorectal cancer and 0.906 (95% CI: 0.845 to 0.967) for breast cancer. The performance of these discriminants was independent of the cancer stage. This study revealed significant differences in plasma amino acid profiles between cancer patients and controls. The development of a cancer alters plasma amino-acid profiles without cachexia or weight loss, and the pattern of change differs between two cancers. Plasma amino-acid profiling might therefore be useful for the early detection of cancer.

Key words: amino acid profiles, plasma, screening, cancer, multivariate analysis

INTRODUCTION

Recent developments in metabolomic approaches enable investigators to measure amino acids and various other metabolites in humans by inexpensive methods with high throughput (Yoshida et al., 2007). Lee et al. (2004) have described how metabolic profiling data can be used to define biological status for diagnostic purposes through multivariate analysis. A great deal of knowledge on human amino-acid metabolism has also been collected over the last three decades through the monitoring of plasma amino-acid levels. Metabolic changes alter the amino-acid balance in patients with various diseases. Because of this, physicians can use indexes such as

*Corresponding author. E-mail: okamoto@gancen.asahi.yokohama.jp. Tel: +81 45 391 5761 ext.4030. Fax: +81 45 366 3157.

Fischer's ratio, that is, the ratio between branched-chain amino acids (BCAAs) and aromatic amino acids (Fisher, 1975, 1976; Rosen, 1977), to track the progression of liver fibrosis and the effectiveness of drug treatment.

The changes in the balance of plasma free amino acids (PFAA) may only be slight during the early stage, whereas later-stage patients may become cachectic due to malnourishment, depending on the deficiency of PFAA (Heber et al., 1985; Mackenzie and Baracos, 2004; Lai et al., 2005).

Investigators can also use post-genomic technologies to derive multivariate functions easily with the aid of a computer. Noguchi et al. (2006) used multivariate functions made up of plasma amino-acid profiles as indexes of diabetes, while Zhang et al. (2006) used them to diagnose liver fibrosis in patients infected with chronic heaptitis C. Shikata et al. (2007), meanwhile, described the structure of the amino-acid metabolism network. The reports by these authors demonstrate that multivariate analysis of plasma free amino-acid profiles is a promising and versatile method for diagnosing various diseases.

Investigators have often found noticeable alterations in the metabolism of cancer cells (Heber et al., 1985; Mackezie and Baracos, 2004; Sido et al., 1998; Rodriguez et al., 2004; Yamaguchi et al., 2005) and changes in the plasma amino-acid profiles of cancer patients (Norton et al., 1985; Naini et al., 1988; Cascino et al., 1991, 1995; Kubota et al., 1991; Lviano et al., 2003; Proenza et al., 2003; Vissers et al., 2005). Cascino et al. (1991, 1995) for example, described significant increases in tryptophan (Trp), glutamic acid (Glu), and ornithine (Orn) in lung cancer patients. Proenza et al. (2003) reported an increased level of Orn in lung cancer patients. Kubota et al. (1991) first used plasma amino-acid profiles to discriminate between breast cancers, gastrointestinal tract cancers, head and neck cancers, and healthy individuals within small sample populations partly made up of malnourished patients. Their results indicated that the amino acid profiles may be useful for cancer diagnosis by site.

The detection of metabolic changes using amino-acid profiles is a promising approach for detecting the presence of various cancers.

Colorectal cancer is a major cause of morbidity and mortality worldwide, and one of the most common causes of cancer deaths in Japan (Saito, 1996). Breast cancer, meanwhile, is the most common cancer among Japanese women (Ohnuki, 2006). Both types of cancer can be eliminated by surgical or endoscopic excision if diagnosed at an early stage, without recurrence or metastases in most patients. The development of technologies for early detection is thus a crucial strategy for decreasing cancer deaths. In this study we investigated differences in the plasma amino-acid profiles between non-cachectic colorectal cancer patients, non-cachectic breast cancer patients, and controls, then examined whether these cancers could be detected by plasma free amino-acid profiling using multivariate analysis.

MATERIALS AND METHODS

Subjects

Sixty-three patients with colorectal cancer and 61 patients with breast cancer diagnosed histologically and hospitalized at the Kanagawa Cancer Center, Yokohama, Japan, between February 2006 and December 2007 were recruited as cases.

The recruitment criteria for the selection of cases were as follows: clinical stage be 0, I, II, or III, no metastasis, tumor marker (CEA, CA19-9, P53) concentrations in serum be under the cut-off levels, and no weight-loss before hospitalization.

All of the patients were fully informed by the chief physician at admission and agreed to participate in this study. One-hundred and fifty-four healthy individuals who had undergone medical examinations at the Center for Multiphasic Health Testing and Services, Mitsui Memorial Hospital, Tokyo, between May and June 2006 were recruited as controls. None of the controls had abnormal tumor markers (CEA, CA19-9).

Of these cases, 49 patients with colorectal cancer and 45 with breast cancer were chosen at random to form the training data set. Age (+/- 5 years)-gender matched controls were chosen for each cancer and the remaining controls were used for a test data set to evaluate the performance of the estimated discriminants. Blood samples were collected from all of the colorectal cancer patients, breast cancer patients, and healthy controls. None of the patients underwent medical interventions such as surgery, chemotherapy, or radiotherapy before their blood was sampled. The baseline characteristics of the patients and controls are summarized in Table 1-A, B.

Analytical methods

Blood samples (5 ml) from all cases and controls were taken from forearm veins after an overnight fast, placed in tubes containing ethylenediaminetetraacetic acid disodium salt (EDTA-2Na; Termo, Japan), and immediately cooled with ice. Blood was drawn from the cancer patients before any operation or treatment. Plasma samples were separated by centrifugation at 3,000 rpm and 4℃ for 15 min, and then stored at −80℃. The plasma samples were deproteinized in a final concentration of 80% acetonitrile before sample preparation. The amino-acid concentrations in the plasma samples were measured by high-performance liquid chromatography (HPLC)-electrospray ionization (ESI)-mass spectrometry (MS), followed by derivatization. An MSQ Plus LC/MS system (Thermo Fischer Scientific, Waltham, MA, USA) equipped with an ESI source was used in positive-ionization mode for selected ion monitoring (SIM). Xcalibur™ version 1.4 SR1 software (Thermo Fisher Scientific, Yokohama, Japan) was used for data collection and processing. The HPLC separation system consisted of an L-2100 pump, L-2200 autosampler, and L-2300 column oven (Hitachi High-Technologies Corporation, Tokyo, Japan). A Wakosil-II 3C8-100HG column (100, 2.1, 3 mm; Wako Pure Chemical Industries, Osaka, Japan) was used for the separation, and the mobile phase consisted of eluent A (25 mM ammonium formate in water) and eluent B (water:acetonitrile = 40:60). The following amino acids and related molecules (24 compounds) were measured and used in the analysis: alanine (Ala), alpha-aminobutyric acid (a-ABA), arginine (Arg), asparagine (Asn), citruline (Cit), glutamic acid (Glu), glutamine (Gln), glycine (Gly), histidine (His), isoleucine (Ile), leucine (Leu), lysine (Lys), methionine (Met), ornithine (Orn), phenylalanine (Phe), proline (Pro), serine (Ser), threonine (Thr), tryptophan (Trp), tyrosine (Tyr), and valine (Val). The plasma levels of amino acids were expressed in μM.

Statistical analysis

The amino-acid concentrations are given as means ± standard

Table 1. The characteristics of the cancer patients and the controls by training/test data.

A) Colorectal cancer patients and controls						
	Training data		Test data		Total	
	Case	Control	Case	Control	Case	Control
Num of data	49	49	13	54	62	103
(Male, Female)	(38,11)	(38,11)	(4,9)	(14,40)	(42,20)	(52,51)
Age (Mean±SD)	64.1±8.2[*]	59.6±5.9	57.5±12.4	55.8±5.7	62.7±9.5[*]	57.6±6.1
(min-max)	(40~78)	(40~69)	(33~75)	(40~69)	(40~78)	(40~69)
BMI (Mean±SD)	23.1±4.3	23.8±4.1	22.2±3.6	22.8±3.0	22.9±3.5	23.3±3.6
(min-max)	(13.8~34.9)	(17.8~42.2)	(13.1~26.9)	(17.4~31.6)	(13.1~34.9)	(17.4~42.2)
Stage0	2	-	0	-	2	-
I	7	-	2	-	9	-
II	19	-	3	-	22	-
III	14	-	8	-	22	-
IV	6	-	0	-	6	-
Uncharacterized	1	-	0	-	1	-
B) Breast cancer patients and controls						
	Training data		Test data		Total	
	Case	Control	Case	Control	Case	Control
Num of data	45	45	16	6	61	51
Age (Mean±SD)	56.4±12.6	57.5±6.0	62.6±9.8	58.3±4.2	58.0±12.1	57.6±5.8
(min-max)	(28~81)	(40~69)	(41~77)	(54~65)	(28~81)	(40~69)
BMI (Mean±SD)	22.0±4.2	22.9±4.2	22.3±3.1	21.8±2.4	22.0±2.9	22.8±4.0
(min-max)	(16.4~30.2)	(17.4~42.2)	(17.0~27.6)	(18.5~25.2)	(16.4~30.2)	(17.4~42.2)
Stage 0	5	-	3	-	8	-
I	22	-	8	-	30	-
II	14	-	4	-	18	-
III	4	-	1	-	5	-
Uncharacterized	0	-	0	-	0	-

[*]:Significant ($p<0.05$) at *t*-test.

deviation (SD). Student's t-tests and Mann-Whitney U-tests were used to assess differences between patients and controls for each cancer. A probability of 5% or less was considered significant. Principal component analysis (PCA) was performed using the standardized z-score for all the training data. Discriminant functions for each cancer were predicted by multiple logistic-regression analysis. The multiple logistic-regression model was applied to all combinations of the 21 amino acids, and the maximum number of variables was restricted to below seven. To avoid multicolinearity, combinations of variables with a variance inflation factor (VIF) exceeding 10 were omitted from the analysis. The best model was defined as the candidate formula with the minimum Akaike's Information Criterion (AIC; Steyerberg et al., 2000). The efficiency of discrimination of the discriminants was estimated from the receiver-operator characteristic (ROC) curve of the estimated probability score of each cancer. The area under the curve (AUC) was calculated for the ROC curve (ROC_AUC; Baker, 2003). To confirm the performance of the estimated discriminants, ROC_AUC values were also calculated using the probability scores obtained from the test data. The Kruskal-Wallis test was used to estimate the effect of the cancer stage on the probability score. All of the statistical and multivariate analyses were performed with MATLAB (The Mathworks, MA, USA) and GraphPad Prism (GraphPad Software, CA, USA).

This study and study protocol were reviewed and approved in advance by the institutional review board of the Kanagawa Cancer Center.

RESULTS

Characteristics of patients and control subjects

The training group included 49 colorectal cancer patients (two at pathological stage 0, seven at stage I, nineteen at stage II, fourteen at stage III, six at stage IV, and one uncharacterized; Table 1A) who had been diagnosed by low-dose helical computed tomography (CT) and biopsy, and 45 breast cancer patients (five at pathological stage 0, twenty-two at stage I, fourteen at stage II, and four at stage III; Table 1B) who had been diagnosed by mammography and biopsy before any symptoms were noticed. There was no significant difference in body-mass index (BMI) between the patients and control subjects for either type of cancer (Table 1A, B).

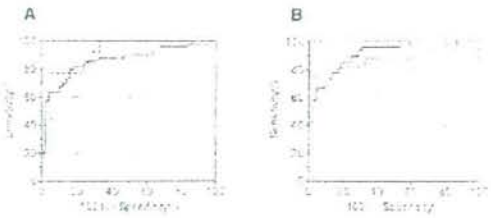

Figure 1. ROC curves of discriminant-1 for colorectal cancer (A) and discriminant-2 for breast cancer (B) of training data (solid line) and test data (dotted line).

Altered amino-acid profiles in colorectal and breast cancers

The plasma concentrations of several amino acids in the colorectal cancer patients were significantly different from those observed in the controls. The levels of Thr, Cit, Val, Met, Ile, Leu, Tyr, and Phe were reduced in the colorectal patients, while that of Glu was increased (Table 2A). The total essential amino acids (EAAs) therefore declined (especially the BCAAs, Val, Leu, and Ile), whereas the total plasma amino acids (SUM AA), including the non-essential amino acids, were unchanged (Table 2A). In contrast, the concentrations of the BCAAs, Tyr, and Phe decreased, whereas the Fischer's ratio (BCAA/(Tyr+Phe); (Rosen et al., 1977) remained unchanged (Table 2A).

The alteration of the plasma amino-acid profile in breast cancer differed from that in colorectal cancer, with fewer changes observed. The levels of Met, Ile, Phe, and Arg decreased in the breast cancer patients, while those of Thr, Ser, Glu, a-ABA and Orn increased (Table 2B). The breast cancer patients were similar to the colorectal cancers in exhibiting no significant change in EAA and BCAA, but they did exhibit an increase in the Fischer's ratio, a change not observed in colorectal cancer (Table 2B).

To summarize the changes of the plasma amino-acid profiles, we performed a principal component analysis (PCA) using the standardized z-score for each amino acid and five principal components (PCs) with eigenvalues of more than 1 (Table 3). To analyze the contributions of three background factors, that is, age, gender, and the presence (=1) or absence (=0) of cancer, to each PC, we used the Spearman's correlation coefficients between these factors and the five PC scores. Our analysis revealed that PC3 was mainly correlated with the presence or absence of colorectal cancer, that PC4 was mainly correlated with the presence or absence of breast cancer, and that gender and age contributed principally to PC1 and PC2 (Table 3). These findings suggest that the altered amino-acid profiles would be useful for detecting the onset of these cancers. They also imply that the two kinds of cancer have different effects on the plasma amino-acid profile.

Multivariate functions for discriminating colorectal and breast cancers

The above-mentioned results suggest that it should be possible to improve discrimination by deriving multivariate functions with the amino-acid profiles as explanatory variables. Noting this, we performed multiple logistic-regression analyses with selected variables using each training datum (as described in the Subjects and Methods section). For colorectal cancer, discriminant-1 consisted of the six amino acids Val, Glu, Thr, a-ABA, Gln, and Pro. For breast cancer, discriminant-2 consisted of the six amino acids Thr, Ala, a-ABA, Ile, Orn, and Arg. The estimated coefficients, standard errors, and p-values for each model are summarized in Table 4.

To evaluate the performance of the discriminants, we calculated ROC curves for each of the discriminant scores. When using training data for this calculation, we obtained ROC_AUC values of 0.860 (95% confidence interval: 0.784 to 0.937) for colorectal cancer and 0.906 (95% confidence interval: 0.845 to 0.967) for breast cancer (Figure 1A and B, solid lines). To confirm the performance of the discriminants, we derived ROC curves from the split test data. These reproduced the good diagnostic performance, with values of 0.910 (95% confidence interval: 0.834 to 0.986) for colorectal cancer, and 0.865 (95% confidence interval: 0.765 to 1.000) for breast cancer (Figure 1A and B, broken lines).

Discriminant scores are independent of cancer stage

If the above-mentioned discriminants are to be used in diagnosis for early cancers, they must have adequate predictive power. To determine whether they met this condition, we compared all of the predicted values (both the training data and test data) of each discriminant with the pathological stage (Figure 2A and B). In the case of colorectal cancer, about 60% of the patients were categorized as early stage (stages 0, I, and II, Table 1A). The Kruskal-Wallis test revealed no significant correlation between the probability of colorectal cancer and the pathological stage (Figure 2A). In the case of breast cancer included training and test data, most of the patients were categorized as early stage (stages 0, I, and II, Table 1B) and only five of the patients were defined as advanced stage (stage III, Table 1B). The discriminant score in the stage 0 or I group was not significantly different from those in the stage II or III groups (Figure 2B). These results suggest that the discriminants obtained are equally predictive for early and later stage.

DISCUSSION

Cancer-associated cachexia is a well known cause of alterations in the plasma amino-acid profiles of cancer

Table 2. The differences of plasma amino-acid profiles between colorectal cancer patients (A), breast cancer patients (B), and controls using the Mann-Whitney U-test.

A) Colorectal cancer			
Amino acids	**Case (mean±SD)**	**Control (Mean ± SD)**	**Significance**
Thr	102.1 ± 23.8	116 ± 23.8	$p<0.01$
Ser	115.8 ± 16.8	121.6 ± 23.4	
Asn	42.1 ± 7.3	45.3 ± 9.5	
Glu	45 ± 18.6	36.9 ± 13.2	$p<0.05$
Gln	596.7 ± 83.9	590.1 ± 94.4	
Pro	163.3 ± 41.7	164.2 ± 39	
Gly	243.2 ± 49.2	251.3 ± 57.6	
Ala	391.8 ± 111	378.4 ± 86.5	
Cit	21.5 ± 4.8	24.4 ± 4.9	$p<0.01$
a-ABA	20.5 ± 7.3	19.1 ± 6	
Val	243.5 ± 50.6	276.8 ±46.1	$p<0.01$
Met	28.1± 5.3	31.4 ± 5.7	$p<0.01$
Ile	68.9 ± 13.3	80.9 ± 16.2	$p<0.001$
Leu	119.8 ± 23.3	136.1 ± 24	$p<0.001$
Tyr	77.5 ± 20.4	84.2 ± 13.6	$p<0.01$
Phe	63.1 ± 11.7	72 ± 10.8	$p<0.001$
His	77.2 ± 17.7	80.3 ± 14	
Trp	59.4 ± 9.8	62.2 ± 12.1	
Orn	56.9 ± 18	59.5 ± 15.6	
Lys	214.3 ± 34.5	217.4 ± 30.6	
Arg	101.2 ± 19	107.6 ± 25	
SUM AA	2851.8 ± 357	2956 ± 255.7	
EAA	976.4 ± 141.5	1073 ± 134.7	$p<0.01$
BCAA	432.2 ± 79.3	493.8 ± 81.5	$p<0.01$
Fisher ratio	3.1 ± 0.5	3.2 ± 0.4	
B) Breast cancer			
Amino acids	**Case (Mean ± SD)**	**Control (Mean ± SD)**	**Significance**
Thr	119.7 ± 22.8	111.5± 25.2	$p<0.05$
Ser	126.4 ± 26.9	114.5 ± 21.4	$p<0.05$
Asn	42.4 ± 7.1	43.6 ± 8.6	
Glu	34.1 ± 14.3	24.3 ± 10.9	$p<0.001$
Gln	594.5 ± 97.1	591.9 ± 75.3	
Pro	146.3 ± 32.9	150.6 ± 38.2	
Gly	291.6 ± 80.6	270.8 ± 75.1	
Ala	395.6 ± 81.4	373.3 ± 93.1	
Cit	19.6 ± 4.7	21.8 ± 5.1	
a-ABA	20 ± 5	17.2 ± 4.4	$p<0.05$
Val	237.2 ± 39	235.5 ± 45.5	
Met	24.9 ± 5.3	26.7 ± 4.3	$p<0.05$
Ile	55.2 ± 12.5	64.8 ± 15.9	$p<0.01$
Leu	108.5 ± 17	115.6 ± 25	
Tyr	69.6 ± 12.4	75.8 ± 15	
Phe	60.6 ± 12.1	68 ± 12.1	$p<0.01$
His	78.3 ± 15.1	82 ± 11.8	
Trp	57.8 ± 9.9	62.2 ± 12.2	
Orn	61.7 ± 17.1	49.4 ± 13.4	$p<0.001$
Lys	205.1 ± 34.8	205.5 ± 29.7	
Arg	90 ± 23.8	107.3 ± 19.4	$p<0.001$

Table 2B Contd.

SUM AA	2839.2 ± 285.9	2812.1 ± 264.7	
EAA	947.4 ± 104.4	971.7 ± 126.5	
BCAA	400.9 ± 61.3	415.8 ± 82.6	
Fisher ratio	3.1 ± 0.4	2.9 ± 0.3	$p<0.05$

Table 3. Correlation between subjects and PCA of the amino-acid profiles in the training data.

Principal components			PCA1	PCA2	PCA3	PCA4	PCA5
Eigenvalue (% of total variance)			6.2	2.9	1.6	1.5	1.1
			29.50%	13.80%	7.60%	7.00%	5.20%
Spearman's correlation coefficient	Gender		-0.3293	0.3515	0.0775	-0.1224	-0.0485
	Age		0.0084	-0.1116	0.0486	0.1039	0.2349
	Presence (=1) or absence (=0) of;						
		Colorectal cancer	-0.0635	-0.1368	0.229	-0.0501	-0.0563
		Breast cancer	-0.1748	0.2117	0.1402	-0.2416	0.0109

Table 4. The estimated coefficients, standard errors, and p-values for each model.

	Coefficient	SE	*p* value
A) Colorectal cancer			
Constant	-0.898	3.034	0.767
Val	-0.042	0.011	0.000
Glu	0.096	0.025	0.000
Thr	-0.039	0.017	0.023
a-ABA	0.177	0.056	0.002
Gln	0.009	0.004	0.027
Pro	0.018	0.009	0.041
B) Breast cancer			
Constant	3.714	3.021	0.219
Thr	0.045	0.021	0.031
Ala	0.010	0.005	0.048
a-ABA	0.210	0.090	0.020
Ile	-0.120	0.039	0.002
Orn	0.061	0.025	0.016
Arg	-0.133	0.037	0.000

patients (Heber et al., 1985; Mackenzie and Baracos patients., 2004; Lai et al., 2005). Cachectic characteris-tics are thought to result from semi-starvation, decreased muscle protein synthesis, increased muscle protein degradation, increased protein synthesis and turnover, increased gluconeogenesis, and other processes (Heber et al., 1985; Mackenzie and Baracos, 2004). Given the possible effects of colorectal cancer on the absorption of amino acids and other nutrients, some suspect that the plasma amino-acid concentrations, particularly those of EAAs, may decrease even when no weight loss is detected (Table 1A, B). It thus appears that the change of plasma amino-acid profiles observed in colorectal cancer may result in part from malnutrition. Indeed, plasma amino-acid profiles are also altered in patients with inflammatory bowel disease (IBD; Papadia et al., 2007). Several studies, however, have demonstrated significant changes in the plasma amino-acid profiles of cancer patients without cachexia (Cascino, 1995; Proenza, 2003; Vissers, 2005). This suggests that multivariate analysis of amino-acid profiles may be useful for the early detection of cancer.

This work therefore recruited the earlier-stage cancer cases before clinical stage IV, although we also included 6 patients with colorectal cancer of pathological stage IV (Table 1).

Our group found no apparent signs of cachexia in the patients of the current study, as none of them had lost significant amounts of body weight (Table 1A, B). We thus speculate that the changes in the amino-acid profiles of breast cancer patients cannot be accounted for by malnutrition or cachexia. Vissers et al. (2005) observed decreases in the plasma levels of several amino acids in breast cancer patients and colon cancer patients with little or no weight loss. These findings suggest that the differences in amino-acid profiles observed are due not to malnutrition, but to cancer-specific alterations of amino-acid metabolism, especially in cases of breast cancer.

There has recently been accumulating evidence of important effects on Arg levels in association with activities of the immune system in cancer patients. Several reports on cancer have mentioned increased production of arginase I, which catalyzes the conversion of Arg into Orn and urea, and increased production of NO synthase, which catalyzes the conversion of Arg into Cit and nitric oxide (NO) (Sido et al., 1998; Rodriguez et al., 2004; Yamaguchi et al., 2005; Vissers et al., 2005). Cascino et al. (1995) reported a decrease in the plasma Arg level and an increase in the Orn level in breast and lung cancers, albeit not to statistically significant degrees. Our group also found a slight, less than significant, decrease of plasma Arg levels in both cancer types examined (Table 2A, B). Based on this finding, we incorporated Arg

into our logistic-regression model for breast cancer (Table 3).

In addition to the possible immunological effects, there is evidence that cancers originating from different organs might lead to different alterations of the amino-acid profile (Norton et al., 1985; Naini et al., 1988; Cascino et al., 1991, 1995; Kubota et al., 1991; Lviano et al., 2003; Proenza et al., 2003; Vissers et al., 2005). The altered plasma amino-acid profiles identified in our study differed between colorectal and breast cancers. As amino acids are produced and assimilated in an organ-specific manner, we were encouraged to find that the indices screened for the two cancers differed in the compositions of the plasma amino acids.

In general, histological diagnostic methods such as colonoscopy and biopsy are established means for obtaining definite diagnoses. Yet the invasiveness and considerable expense render them unfeasible for many individuals who undergo medical examinations. Instead, faecal occult blood testing is used to screen for colorectal cancer (Saito, 1996) and mammography is used to screen for breast cancer (Ohnuki et al., 2006; Moss et al., 2006). Both of these methods have disadvantages. In faecal occult blood testing, for example, the appearance of haemoglobin in stool is not specific for neoplasms (Ito et al., 2002). Mammography, meanwhile, exposes individuals to radiation and would not be cost-effective for annual examination (Ohnuki et al., 2006). Even if no one test is invasive or expensive, a battery of various tests performed in an annual medical examination can be burdensome and expensive. The discovery of new tumor markers using genomic and proteomic technologies is being pursued vigorously (Cho, 2007). Yet few, if any, of the markers identified so far are sensitive or specific enough to be clinically useful for early detection. To name just two examples, the major tumor marker for colorectal cancer, carcinoembryonic antigen (CEA), and the major marker for breast cancer, cancer antigen 15-3 (CA15-3), are both thought to lack adequate sensitivity for early detection (Ito et al., 2002; Cho, 2007).

Nevertheless, the results presented here demonstrate that plasma free amino-acid profiling is useful for detecting both colorectal cancer and breast cancer. Unlike conventional tumor markers, the discriminants developed in this study identify patients equally well at any stage of cancer. Thus, they may used for screening.

This study had important limitations. First, the samples were limited in number, particularly those for testing data, and they were taken from only two cancer sites. Second, the number of cases was too low to permit analyses of confounding factors such as sex, age, liver disease, and other chronic diseases. Third, the study was not a randomized controlled case-control study and a cohort study, but a non randomized controlled study. Hereafter, we will be planning a randomized controlled cohort study to establish a new cancer screening method with plasma free amino acid profiles.

If it ever becomes possible to evaluate the incidence of every type of cancer using only one plasma sample, the reduction in cancer mortality will be tremendous.

ACKNOWLEDGEMENTS

This work has been supported by a Grant-in-Aid for Scientific Research on Basic Research B (No. 17390195) from the Ministry of Education, Culture, Sports, Science and Technology of Japan. We thank Dr. H Miyano, Mr. K. Shimbo, Mr. H. Yoshida, Ms. M. Amao, and Ms. M. Nakamura for amino-acid analyses. We also thank Ms. T. Kasakura and Ms. Y. Osawa for data acquisition.

REFERENCES

Baker SG (2003). The central role of receiver operating characteristic (ROC) curves in evaluating tests for the early detection of cancer. J. Nat. Cancer Inst. 95: 511-515.

Cascino A, Cangiano C, Ceci F (1991). Increased plasma free tryptophan levels in human cancer; a tumor related effect? Anticancer Res. 11: 1313-1316.

Cascino A, Muscaritoli M, Cangiano C (1995). Plasma amino acid imbalances in patients with lung and breast cancer. Anticancer Res. 15: 507-510.

Cho WCS (2007). Contribution of oncoproteomics to cancer biomarker discovery. Mol. Cancer. 6: 25-37.

Fischer JE, Funovics JM, Aguirre A (1975). The role of plasma amino acids in hepatic encephalcopathy. Surgery. 78: 276-290.

Fischer JE, Rosen HM, Ebeid AM, James JH, Keane JM, Soeters PB (1976). The effect of normalization of plasma amino acids on hepatic encephalcopathy in man. Surgery 80: 77-91.

Heber D, Byerly LO, Chlebowski RT (1985). Metabolic abnormalities in cancer patient. Cancer 55: 225-229.

Ito S, Hibi K, Nakayama H (2002). Detection tumor DNA in serum of colorectal cancer patients. Jpn. J. Cancer Res. 93:1266-1269.

Kubota A, Meguid MM, Hitch DC (1991). Amino acid profiles correlate diagnostically with organ site in three kinds of malignant tumors. Cancer 69: 2343-2348.

Lai HS, Lee JC, Lee PH (2005). Plasma free amino acid profile in cancer patients. Seminars in Cancer Biol. 15: 267-276.

Lee K, Hwang D, Yokoyama T (2004). Identification of optimal classification functions for biological sample and state discrimination from metabolic profiling data. Bioinformatics 20: 959-969.

Lviano A, Cascino A, Muscaritoli M, Fanfarillo F, Fanelli R (2003). Tumor induced changes in host metabolism: a possible role for free tryptophan as a marker of neoplastic disease. Adv. Exp. Med. Biol. 527: 363-366.

Mackenzie M, Baracos VE (2004). Cancer associated cachexia: altered metabolism of protein and amino acids. In: Cynober LA editor. Metabolic and therapeutic aspects of amino acids in clinical nutrition. FL: CRC Press. pp. 339-354.

Moss SM, Cuckle H, Evans A, Johns L, Waller M, Bobrow L (2006). Effect of mammographic screening from age 40 years on breast cancer mortality at 10 year's follow-up: a randomised controlled trial. Lancet 368: 2053-2060.

Naini AB, Dickerson JWT, Brown MM (1988). Preoperative and postoperative levels of plasma protein and amino acid in esophageal and lung cancer patients. Cancer 62: 355-360.

Noguchi Y, Zhang QW, Sugimoto T (2006). Network analysis of plasma and tissue amino acid and the generation of an amino index for potential diagnostic use. Am. J. Clin. Nutr. 83: 513S-519S.

Norton JA, Gorchboth CM, Wesley RA, Burt ME, Brennan MF (1985). Fasting plasma amino acid levels in cancer patients. Cancer 56: 1181-1186.

Ohnuki K, Kuriyama S, Shoji N, Nishino Y, Tsuji I, Ohuchi N (2006). Cost-effectiveness analysis of screening modalities for breast cancer in Japan with special reference to women aged 40-49 years. Cancer Sci. 97: 1242-1247.

Papadia C, Shereood RA, Kalantzis C (2007). Plasma citrulline con-

centration: a reliable marker of small bowel absorptive capacity independent of intestinal inflammation. Am. J. Gastroenterol. 102: 1474-1482.
Proenza AM, Olivier J, Palou A, Roca P (2003). Breast and lung cancer are associated with a decrease in blood cell amino acid content. J. Nutr. Biochem. 14: 133-138.
Rodriguez PC, Quiceno DG, Zabaleta J (2004). Arginase I production in the tumor microenvironment by mature myeloid cells inhibits T-cell receptor expression and antigen-specific T-cell responses. Cancer Res 64: 5839-5849.
Rosen HM, Yoshimura N, Hodgman JM, Fischer JE (1977). Plasma amino acid patterns in hepatic encephalcopathy of differing etiology. Gastroenterol. 72: 483-487.
Saito H (1996). Screening for colorectal cancer by immunochemical focal occult blood testing. Jpn. J. Cancer Res. 87: 1011-1024.
Shikata N, Maki Y, Noguchi Y (2007). Multi-layered network structure of amino acid (AA) metabolism characterized by each essential AA-deficient condition. Amino acids. 33: 113-1121.
Sido B, Hack V, Hochlehnert A, Lipps H, Herfarth C, Drage W (1998). Impairment of intestinal glutathione synthesis in patients with inflammatory bowel disease. Gut. 42: 485-482.
Steyerberg EW, Eijkemans MJC, Harrell Jr FE, Habbema JDF (2000). Prognostic modelling with logistic regression analysis: a comparison of selection and estimation method in small data sets. Stat. Med. 19: 1059-1079.
Vissers YLJ, Dejong CHC, Luiking YC, Fearon LCH, von Meyenfeldt MF, Deutz NEP (2005). Plasma arginine concentration are reduced in cancer patients: evidence for arginine deficiency? Am. J. Clin. Nutr. 81: 1142-1146.
Yamaguchi K, Saito H, Oro S, Tatebe S, Ikeguchi M, Tsujitani S (2005). Expression of inducible nitric oxide synthase is significantly correlated with expression of vascular endothelial growth factor and dendritic cell infiltration. Oncology 68: 471-478.
Yoshida M, Mizukoshi T, Hirayama K, Miyano H (2007). Comprehensive analytical method for the determination of hydrophilic metabolites by high-performance liquid chromatography and mass spectrometry. J. Agric. Food Chem. 53: 551-560.
Zhang Q, Takahashi M, Noguchi Y (2006). Plasma amino acid profiles applied for diagnosis of advanced liver fibrosis in patient with chronic hepatitis C infection. Hepatol. Res. 34: 170-177.

THE JOURNAL OF BIOLOGICAL CHEMISTRY VOL. 283, NO. 51, pp. 35805–35814, December 19, 2008

Nuclear Inhibitor of Protein Phosphatase-1 (NIPP1) Directs Protein Phosphatase-1 (PP1) to Dephosphorylate the U2 Small Nuclear Ribonucleoprotein Particle (snRNP) Component, Spliceosome-associated Protein 155 (Sap155)*[S]

Received for publication, July 17, 2008, and in revised form, October 1, 2008 Published, JBC Papers in Press, October 8, 2008, DOI 10.1074/jbc.M805468200

Nobuhiro Tanuma[‡§1], **Sei-Eun Kim**[§2], **Monique Beullens**[¶], **Yao Tsubaki**[§], **Shinya Mitsuhashi**[§‖], **Miyuki Nomura**[‡], **Takeshi Kawamura**[**], **Kyoichi Isono**[‡‡], **Haruhiko Koseki**[‡‡], **Masami Sato**[‡], **Mathieu Bollen**[¶], **Kunimi Kikuchi**[§], **and Hiroshi Shima**[‡3]

From the [‡]*Division of Cancer Chemotherapy, Miyagi Cancer Center Research Institute, Natori 981-1293, Japan,* [§]*Division of Biochemical Oncology and Immunology, Institute for Genetic Medicine, and* [‖]*Division of Applied Bioscience, Research Faculty of Agriculture, Hokkaido University, Sapporo 060-0815, Japan,* [¶]*Laboratory of Biosignaling and Therapeutics, Department of Molecular Cell Biology, Faculty of Medicine, KULeuven, Leuven B-3000, Belgium,* [**]*Laboratory for Systems Biology and Medicine, RCAST, The University of Tokyo, Tokyo 153-8904, Japan, and* [‡‡]*RIKEN Research Center for Allergy and Immunology, Yokohama 230-0045, Japan*

Pre-mRNA splicing entails reversible phosphorylation of spliceosomal proteins. Recent work has revealed essential roles for Ser/Thr phosphatases, such as protein phosphatase-1 (PP1), in splicing, but how these phosphatases are regulated is largely unknown. We show that nuclear inhibitor of PP1 (NIPP1), a major PP1 interactor in the vertebrate nucleus, recruits PP1 to Sap155 (spliceosome-associated protein 155), an essential component of U2 small nuclear ribonucleoprotein particles, and promotes Sap155 dephosphorylation. C-terminally truncated NIPP1 (NIPP1-ΔC) formed a hyper-active holoenzyme with PP1, rendering PP1 minimally phosphorylated on an inhibitory site. Forced expression of NIPP1-WT and -ΔC resulted in slight and severe decreases in Sap155 hyperphosphorylation, respectively, and the latter was accompanied with inhibition of splicing. PP1 overexpression produced similar effects, whereas small interfering RNA-mediated NIPP1 knockdown enhanced Sap155 hyperphosphorylation upon okadaic acid treatment. NIPP1 did not inhibit but rather stimulated Sap155 dephosphorylation by PP1 *in vitro* through facilitating Sap155/PP1 interaction. Further analysis revealed that NIPP1 specifically recognizes hyperphosphorylated Sap155 thorough its Forkhead-associated domain and dissociates from Sap155 after dephosphorylation by associated PP1. Thus NIPP1 works as a molecular sensor for PP1 to recognize phosphorylated Sap155.

Pre-mRNA splicing is an essential step for expression of most genes in metazoans. Intron excision from a nascent transcript is achieved by pre-mRNA splicing catalyzed by the spliceosome, a macromolecular complex consisting of five small nuclear ribonucleoprotein particles (snRNPs)[4] and a large number of non-snRNP proteins. Spliceosome assembly is an ordered process that includes stepwise recruitment of U1, U2, U5, and U4/6 snRNPs on a pre-mRNA and sequential formation of complex E → A/B → B* → C. The activated B* spliceosome catalyzes step I of splicing, whereas the C complex catalyzes step II. During and after splicing, spliceosome components dissociate and are recycled for further rounds of splicing. Spliceosome assembly/disassembly and splicing catalysis are thought to be regulated in part by reversible phosphorylation of spliceosomal proteins (1–3).

U2 snRNP includes U2 snRNA and two heteromeric protein complexes, Sf3a and Sf3b. Sap155, also known as Sf3b1 or Sf3b155, is a component of the Sf3b and becomes hyperphosphorylated concomitant with or just after the first catalytic step of splicing *in vitro* (4). A recent study reveals that Sf3a/b proteins are destabilized and dissociate from the RNP core of the activated spliceosome during the transition from the B to C complex (5). Although Sf3a and Sf3b are essential early in the splicing reaction, they are apparently not required for the second catalytic step. Currently, it is not known what triggers exchange of proteins during spliceosome transitions.

Shi *et al.* (6) reported that the protein Ser/Thr phosphatase (PPase) type 1 (PP1) and/or type 2A (PP2A) are essential for splicing *in vitro*, in particular, at the second catalytic step. They also observed that Sap155 and U5-116k are potential substrates of these two PPases, suggesting the importance of dephosphorylation of spliceosomal proteins in spliceosome structural

* This work was supported in part by grants-in-aid for scientific research (B and C) provided by the Japan Society for the Promotion of Science of Japan. The costs of publication of this article were defrayed in part by the payment of page charges. This article must therefore be hereby marked "*advertisement*" in accordance with 18 U.S.C. Section 1734 solely to indicate this fact.

[S] The on-line version of this article (available at http://www.jbc.org) contains supplemental Figs. 1–3.

[1] To whom correspondence may be addressed. Fax: 81-22-3811196; E-mail: tanuma-no872@pref.miyagi.jp.

[2] Present address: Clinical Research Team, Hanmi Pharm. Co. Ltd., Seoul, Korea.

[3] To whom correspondence may be addressed: 47-1 Nodayama, Medeshima-Shiode, Natori 981-1293, Japan. Fax: 81-22-3811196; E-mail: shima-hi632@pref.miyagi.jp.

[4] The abbreviations used are: snRNP, small nuclear ribonucleoprotein particle; RNP, ribonucleoprotein; PP1, protein phosphatase-1; NIPP1, nuclear inhibitor of PP1; siRNA, small interfering RNA; PBS, phosphate-buffered saline; Dox, doxycycline; RNAi, RNA interference; OA, okadaic acid; PPase, phosphatase; HTO, HeLa-Tet-Off; RPA, RNase protection assay; FHA, Forkhead-associated; RT, reverse transcription; FHA, Forkhead-associated.

rearrangement. However, how PP1 and PP2A regulate phosphorylation of spliceosomal proteins is not well understood.

Both PP1 and PP2A are often targeted to specific substrates by binding partners. For example, PP1 is regulated *in vivo* primarily by interaction with various regulatory subunits that dictate subcellular localization, substrate specificity, or enzymatic activity (7). In some cases, regulatory subunits are phosphorylated/dephosphorylated, resulting in activity changes that modulate PP1 activity in response to environmental cues such as hormones and second messengers (8–10). In addition to interacting with regulatory subunits, PP1 is regulated by phosphorylation. Phosphorylation by cyclin-dependent kinases lower PP1 activity *in vitro* and *vivo* in *Schizosaccharomyces pombe* and in human cells (11, 12). The PP1 phosphorylation site is highly conserved among species and has been mapped to the C terminus. Studies in yeast and human cells suggest that PP1 phosphorylation is essential for proper cell cycle progression (13, 14).

A major nuclear interaction partner of PP1 in vertebrate cells is the nuclear inhibitor of PP1 (NIPP1) (7). Targeted disruption of the *Nipp1* gene in mice results in embryonic lethality, indicating an essential role *in vivo* (15). NIPP1 has two PP1 binding regions as follows: a central domain containing a so-called RV*X*F-motif, which represents a high affinity binding motif and a low affinity binding region mapped to the NIPP1 C terminus (16, 17). The precise function of the latter interaction is not yet understood. Previous studies suggest the importance of NIPP1 in regulating pre-mRNA splicing. NIPP1 localizes in nuclear speckles, domains rich in splicing machinery components. Several splicing-related proteins such as Cdc5L, SAP155, and MELK have been identified as potential ligands of the Forkhead-associated (FHA) domain of NIPP1 (18–20). FHA is a modular phospho-Thr/Ser recognition motif (21, 22). Beullens and Bollen (23) reported that NIPP1 physically associates with spliceosomes through the FHA domain and that a dominant negative form of NIPP1 blocks the B to C transition of spliceosome assembly in the HeLa cell nuclear extracts by an unknown mechanism. Although there is a report that NIPP1 protein lacking the RV*X*F motif partially compromises splicing *in vitro*, data from splicing assays using HeLa nuclear extracts are contradictory (23, 24). Thus both the mode of NIPP1 action and the potential role of PP1/NIPP1 interaction in pre-mRNA splicing remain obscure.

To analyze function of NIPP1 in pre-mRNA splicing, we re-evaluated the physical and functional association among pre-mRNA/RNA, NIPP1, and PP1 *in vivo* using cell-based assays. We show that NIPP1 works as a targeting subunit that directs PP1 to dephosphorylate Sap155, not as an inhibitor of PP1. Our results suggest a regulatory mechanism ensuring proper Sap155 phosphorylation-dephosphorylation cycles during pre-mRNA splicing.

MATERIALS AND METHODS

Antibodies—Anti-U5-116k antibody was kindly provided by Dr. H. Brahms and Dr. R. Lührmann (25). Anti-Sap155 (26), anti-Myc 9e10, anti-Cdc5L, anti-FLAG M2, anti-phospho-Thr-320-PP1, anti-MELK, and anti-pan-PP1 E9 antibody were purchased from MBL (Nagoya, Japan), Roche Applied Science, BD Transduction Laboratories, Sigma, Cell Signaling Technology Inc. (Danvers, MA), Abcam (Cambridge, UK), and Santa Cruz Biotechnology Inc. (Santa Cruz, CA), respectively. Antibodies specific to each PP1 isoform have been described (27). Polyclonal or monoclonal anti-NIPP1 antibodies were generated against a peptide corresponding to the C-terminal 20 amino acids in our laboratory or purchased from BD Transduction Laboratories.

Plasmid Constructs—The pTRE-β-globin reporter has been described (28). The BseRI-BstXI region of pTRE-β-globin, encompassing the β-globin gene from the 3′-half of exon 1 to the 5′-half of exon 3, was replaced with a corresponding BseRI-BstXI fragment of β-globin cDNA derived from pTRE-β-globin; the sequence verified, and the resulting plasmid was designated pTRE-intronless-β-globin. Its nucleotide sequence is identical to that of pTRE-β-globin except intron 1 and 2 sequences are excluded. NIPP1 expression plasmids were constructed by subcloning cDNAs encoding wild-type or mutant forms of rat NIPP1 (29) into pCMV-FLAG2 (Sigma). Myc-PP1 constructs are described elsewhere (30).

Cell Culture and Transfection—HeLa-Tet-Off (HTO) cells (Clontech) were cultured in Dulbecco's modified Eagle's medium containing 10% fetal calf serum and 250 μg/ml geneticin. Transfections were done using FuGENE 6 reagent (Roche Applied Science) according to the manufacturer's recommendation. For stable transfection, cDNAs encoding FLAG-tagged wild-type or mutant NIPP1 were subcloned into the pTRE vector (Clontech). HTO cells in 10-cm dishes were transfected with 10 μg of pTRE-NIPP1-WT or -ΔC with 0.5 μg of pTK-Hyg (Clontech). Drug-resistant clones were selected in 200 μg/ml hygromycin, 250 μg/ml geneticin, and 1 μg/ml Dox. Two weeks later, ~150 independent clones for each construct were screened for expression of exogenous NIPP1 by immunoblotting with anti-FLAG antibody. Several clones for each construct (four for WT NIPP1 and three for NIPP1-ΔC) exhibited low and high levels of FLAG-NIPP1 proteins in the presence and absence of Dox, respectively, and were selected for further experiments. After establishment, stable clones were maintained in medium containing 5–10 ng/ml Dox.

In Vitro and in Vivo Splicing Assays—*In vitro* splicing was performed as described (23). RNP immunoprecipitation assays were performed essentially as described (31) with slight modification. Cells were fixed in 0.75% formaldehyde/PBS at room temperature for 10 min, washed twice in PBS, and harvested. Cells were lysed in 1 ml of RIPA buffer (20 mM Tris-Cl, 150 mM NaCl, 5 mM EDTA, 10% glycerol, 0.1% SDS, 1% Triton X-100, and 0.1% deoxycholate) by sonication (Sonifier 450, Branson, Danbury, CT). 50 μl each of lysate was stored on ice as "Input," and the rest was immunoprecipitated with anti-FLAG-agarose beads at room temperature for 2 h. Beads were collected by centrifugation and washed four times with gentle rotation for 5 min, followed by elution of RNPs with FLAG peptide (Sigma). "Inputs" and eluates were heated to 75 °C for 90 min to reverse cross-links and phenol-extracted twice. RNAs were ethanol-precipitated using yeast tRNA and Glyco-blue co-precipitants (Ambion) as carrier and treated with RNase-free DNase (DNA-free turbo, Ambion). RNA was reverse-transcribed using SuperScript III RTase (Invitrogen) using the RT primer 5′-

GTGCAGCTTGTCACAGTGCAG-3′. PCR was undertaken using standard protocols with Ex Taq-HS polymerase (Takara Bio Inc., Otsu, Japan) and the following primers for β-globin: sense, 5′-ATGGTGCATCTGACTCCTGAG-3′; antisense, 5′-ACTAAAGGCACCGAGCACTTTCTTG-3′. To analyze effects of NIPP1 on splicing rates, HTO cells in 10-cm dishes were transfected with 7.5 μg of NIPP1 expression plasmids with 2.5 μg of pTRE-β-globin. Four hours later, cells were split and further cultured without Dox for 20 h. At indicated time points after Dox addition, cells were harvested, and total RNA was isolated for Northern blot analysis with a ^{32}P-labeled β-globin probe. For RPAs, antisense riboprobes complementary to exon 1/intron 1 or exon 2/intron 2 boundaries of β-globin gene were synthesized by *in vitro* transcription using MAXI script (Ambion, Austin, TX) and T7 polymerase. Hybridization and RNase digestions were performed using the RPA III (Ambion) kit according to the manufacturer's instruction. Protected RNAs were subjected to denaturing PAGE and visualized using the FLA system (Fuji Film Co., Tokyo, Japan).

Immunoprecipitation and Western Blot Analysis—Cells were lysed in RIPA or SDS buffer (125 mM Tris-Cl, pH 6.8, 1% SDS) by sonication using a "Bio-ruptor" sonicator (CosmoBio, Tokyo, Japan). For co-immunoprecipitation, cells were lysed in buffer (50 mM Tris-Cl, pH 7.4, 125 mM NaCl, 0.2% Triton X-100, 2 mM EDTA, 1 mM phenylmethylsulfonyl fluoride, leupeptin, and aprotinin) by sonication. Lysates were incubated with anti-FLAG-agarose or anti-Myc-agarose (Sigma) for 3–4 h at 4 °C. Immunocomplexes were collected by centrifugation, washed three times with lysis buffer without protease inhibitors, and immunoblotted.

Immunohistochemistry—Cells grown on collagen-coated coverslips were fixed in PBS containing 3.7% formaldehyde for 10 min. After permeabilization with 0.2% Triton X-100, cells were incubated in PBS containing 5% (w/v) bovine serum albumin and 0.5 μg/ml anti-FLAG M2 monoclonal antibody overnight at 4 °C. Immunoreactants were further visualized using Alexa Fluor488-conjugated anti-mouse IgG secondary antibody (Invitrogen), and images were acquired using a Pascal confocal laser-scanning microscope (Zeiss).

^{32}P-Orthophosphate Labeling—Stable clones were cultured in the presence or absence of 10 ng/ml Dox for 24 h and then in phosphate-free medium (Invitrogen) containing 10% fetal calf serum (dialyzed three times against 100 volumes of Hepes buffer) and ^{32}P-orthophosphate (PerkinElmer Life Sciences) at 1 mCi/ml for an additional 4 h. Cells were harvested, lysed by sonication using the Bio-ruptor sonicating machine, and subjected to immunoprecipitation. Immunoprecipitates were separated by SDS-PAGE, followed by immunoblot analysis and autoradiography using the FLA system.

In Vitro De-phosphorylation Experiments—HTO cells were lysed in buffer (50 mM Tris-Cl, 100 mM NaCl, 2 mM EDTA, 10% EDTA, 0.1% Triton X-100) by sonication. Lysates were incubated with or without either PP1 (a recombinant PP1α isoform; Calbiochem) or NIPP1-PP1 holoenzyme at 30 °C for 10–60 min. The NIPP1-PP1 holoenzyme was constituted by preincubation of recombinant PP1α with His-NIPP1 at several ratios on ice for 20 min in Tris-buffered saline. His-NIPP1 was expressed in *Escherichia coli* using the pET system (Novagen, San Diego, CA) and purified using TALON beads (Clontech) following the manufacturer's recommendations. Sap155 was immunopurified from lysates of HeLa cells treated with 100 nM okadaic acid for 6–8 h using anti-Sap155 monoclonal antibody-conjugated agarose.

Phosphatase Assay—Immunoprecipitates with anti-FLAG-agarose were eluted twice by incubating beads with 200 μg/ml FLAG peptide. Eluates were subjected to a phosphatase assay and Western blotting. PP1 activity measurement was as described (26).

RNAi Experiments—siRNA duplexes against human NIPP1 (Stealth RNAi) were purchased from Invitrogen (HSS143426 and HSS143427). Stealth RNAi Negative control Medium GC duplex (Invitrogen) served as control. siRNA transfection was undertaken using Lipofectamine RNAiMAX (Invitrogen) according to the manufacturer's instructions at final siRNA concentrations of 5 nM in culture.

Overlay Assay—Sap155 was immunoprecipitated from HeLa cell lysates treated with 100 nM okadaic acid (OA) for 6–8 h, separated by SDS-PAGE, and transferred to a nitrocellulose membrane. The membrane was blocked with 5% bovine serum albumin in PBS and reacted with solutions supplemented with phosphatase inhibitors (Roche Applied Science) at 4 °C for 1 h. Membranes were washed with PBS, 0.1% Tween plus phosphatase inhibitors at 4 °C for 5 min twice and then UV-irradiated to fix complexes.

Statistical Analysis—One-way analysis of variance combined with Tukey's test was used to analyze data with unequal variance between each group. A probability level of 0.05 was considered significant.

RESULTS

Physical and Functional Interaction between NIPP1 and Pre-mRNA Splicing in Intact Cells—To elucidate interaction between NIPP1 and the spliceosome *in vivo*, we performed an RNP immunoprecipitation assay (31). Cells transfected with FLAG-NIPP1 (Fig. 1*A*) together with the β-globin reporter plasmid pTRE-β-globin were treated with formaldehyde, recovered, and lysed. RNPs containing FLAG-NIPP1 were immunoprecipitated using an anti-FLAG antibody. The cross-links were reversed, and the immunoprecipitated RNAs were detected by RT-PCR ("Minus RT" controls are presented as supplemental Fig. 1). As shown in Fig. 1*B*, both unspliced and spliced β-globin RNAs co-immunoprecipitated with FLAG-NIPP1-WT. We next examined interaction between NIPP1 mutants (Fig. 1*A*) and β-globin pre-mRNA/mRNAs. Similar results were obtained with NIPP1-R53A, which has a nonfunctional FHA domain (Fig. 1*C*). NIPP1-V201A/F203A (NIPP1-RATA), which is deficient in PP1 binding (Fig. 1*D*), reproducibly co-immunoprecipitated pre-mRNA more efficiently than did NIPP1-WT. NIPP1-ΔC, which lacks the C-terminal 22 amino acids constituting a second PP1-binding region, interacted almost exclusively with unspliced pre-mRNA. This observation correlated with accumulation of unspliced reporter pre-mRNA in cell lysates, as detected by RT-PCR ("total RNA" in Fig. 1*B*), suggesting inhibition of splicing by that mutant form of NIPP1. Because transcription and "post-transcriptional" RNA processing are functionally coupled (32), the

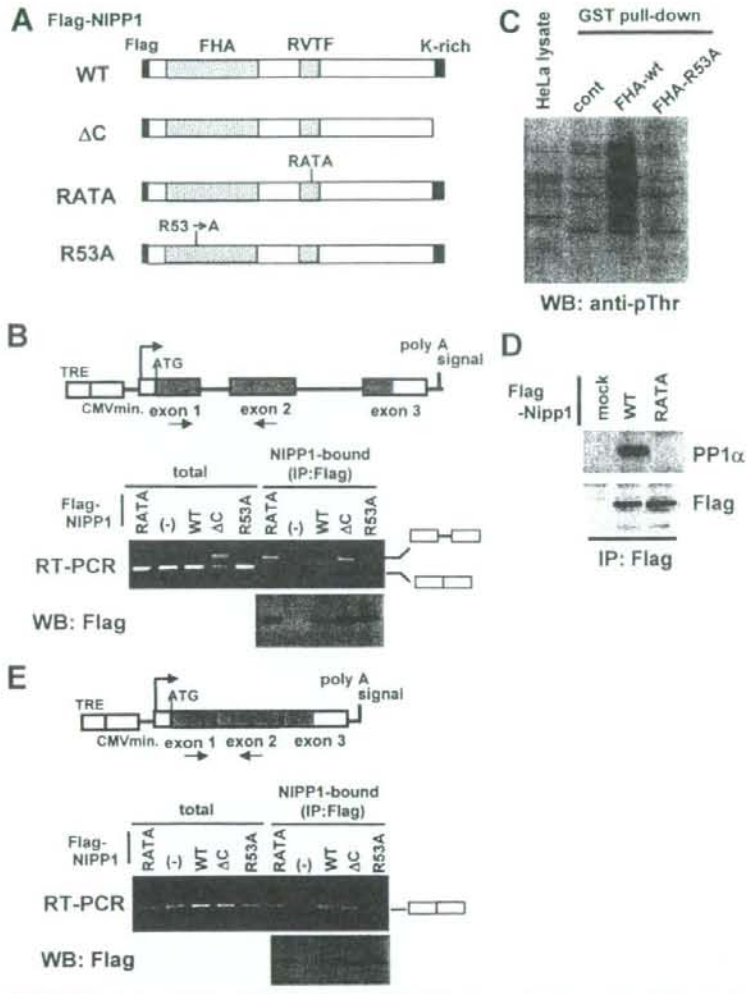

FIGURE 1. **Physical association of NIPP1 and pre-mRNA/mRNA of β-globin reporter genes in intact cells.** *A*, NIPP1 mutant proteins used in this study. Each is N-terminally tagged with the FLAG epitope. The FHA domain and PP1-binding region containing RVTF sequence and Lys (*K*)-rich region of NIPP1 are shown. *B*, *in vivo* interaction between NIPP1 and β-globin reporter pre-mRNA/mRNA. Structure of the human β-globin gene reporter construct, pTRE-β-globin, is shown on the *top*. The open reading frame is represented by *shaded boxes*, and introns and vector stuffer sequences are represented by *lines*. *Arrows* indicate position of primers used in RT-PCR analysis. HTO cells were transiently transfected with FLAG-NIPP1 expression vector with the β-globin reporter plasmid. About 24 h after transfection, cells were subjected to RNP immunoprecipitation assay. Co-immunoprecipitated reporter pre-mRNA/mRNAs with FLAG-NIPP1 were detected by RT-PCR. Positions of amplified DNA fragments derived from unspliced pre-mRNA and spliced mRNA are shown at *right*. Levels of immunoprecipitated FLAG-NIPP1 proteins were also assessed by immunoblotting (*WB*). *C*, pulldown experiments were performed using GST-tagged FHA domains of NIPP1. GST, GST-FHA-WT, or GST-FHA-R53A was mixed with whole cell lysates of HeLa cells. Co-precipitated proteins were subjected to immunoblotting using anti-phospho-Thr antibody. *Cont*, control. *D*, HeLa-TetOff cells were transiently transfected with NIPP1-WT or NIPP1-RATA, lysed, and subjected to immunoprecipitation (*IP*) using an anti-FLAG antibody. Immunoblots were performed using anti-PP1α or anti-FLAG antibodies. *E*, effects of wild-type and mutant forms of NIPP1 on mRNA of an intron-less β-globin reporter gene. Structure of the intron-less human β-globin reporter construct is at the *top*. Interaction between NIPP1 and the intron-less reporter mRNA was analyzed as in *B*.

effects of NIPP1-ΔC on splicing might represent an indirect transcriptional effect. To distinguish between these possibilities, we repeated the assays using a corresponding intron-less reporter gene. As shown in Fig. 1*E*, NIPP1-ΔC and other NIPP1 constructs did not significantly affect mRNA levels of the intron-less reporter, suggesting that the effect of NIPP1-ΔC on splicing is specific for a splicing-related event(s) or for splicing itself. Intriguingly, all NIPP1 variants co-precipitated mRNA derived from the intron-less reporter, consistent with a recent report that the U2 snRNP is recruited to both intron-containing transcripts and transcripts of intron-less genes, such as histone genes, to facilitate 3′-processing (33).

To further delineate effects of mutant NIPP1, we took advantage of the pTRE-β-globin reporter, in which the transcription is regulated by a TRE sequence upstream of the cytomegalovirus promoter (Fig. 1*B*). When introduced into cells expressing the Tet-repressor (Tet-Off cell lines), *de novo* transcription from the reporter is specifically and rapidly suppressed by the stable tetracycline analogue Dox (28). Northern blot analysis showed that expression of NIPP1-ΔC decreased steady-state levels of β-globin mRNA, whereas expression of NIPP1-WT had produced little if no effect (Fig. 2*A*). A band likely representing β-globin pre-mRNA (indicated by *asterisk* in Fig. 2*A*) migrated more slowly than β-globin mRNA and was more abundant in cells transfected with NIPP1-ΔC compared with mock- or NIPP1-WT-transfected cells. To confirm this observation, we performed an RPA (Fig. 2*C*; see supplemental Fig. 2 for assay design) and found that in mock-transfected cells levels of unspliced β-globin pre-mRNA were rapidly decreased after Dox-mediated block of *de novo* transcription of the reporter gene, as seen in Fig. 2*C*. This decrease is likely due to splicing of the reporter pre-mRNA. Strikingly, unspliced pre-mRNA was more abundant in cells transfected with NIPP1-ΔC, whereas mature spliced mRNA levels were decreased (Fig. 2*C*). Additionally, the half-life of unspliced pre-mRNA in NIPP1-ΔC-transfected cells appeared much longer than that seen in mock- and NIPP1-WT-transfected cells

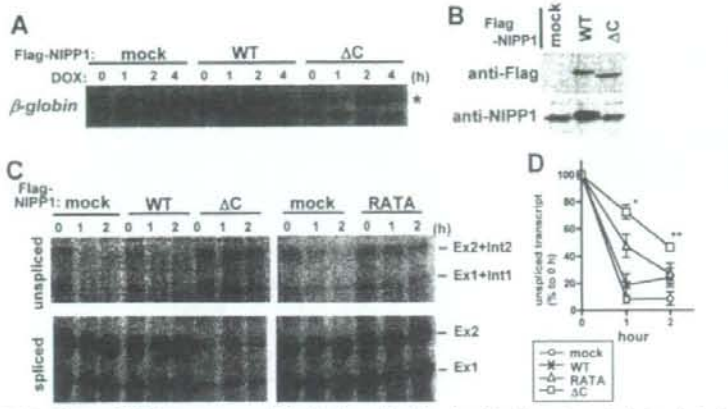

FIGURE 2. **Effects of NIPP1 mutants on splicing *in vivo* and *in vitro*.** *A* and *B*, cells were transiently transfected with FLAG-NIPP1 expression vector and the pTRE-β-globin plasmid. After 24 h, cells were harvested at indicated time points after addition of 10 ng/ml Dox to the medium. Total RNA was isolated and analyzed by Northern blotting with β-globin cDNA (*A*). The lysates of cells at time 0 were analyzed by Western blotting using the anti-FLAG (*upper*) and anti-NIPP1 antibody, which recognizes the Lys-rich region of NIPP1 (*lower*) (*B*). *C* and *D*, decay of unspliced pre-mRNA after the shut-off of *de novo* transcription. Cells were transiently transfected, treated with Dox, and harvested as in *A*. Total RNA was isolated and analyzed by a multiprobe RPA (*C*). Migration of protected fragments derived from unspliced and spliced mRNAs is shown. Band intensities derived from the unspliced transcript were evaluated and are shown as values relative to those at 0 h (*D*). Data represent mean values of 3–4 independent RPAs with S.D. *, $p < 0.001$; **, $p < 0.01$ (Δ*C versus* WT).

(Fig. 2*D*). As described, NIPP1-RATA associated with unspliced pre-mRNA more efficiently than did NIPP1-WT, whereas NIPP1-RATA did not accumulate unspliced pre-mRNA, in contrast to NIPP1-ΔC (Fig. 1*B*). It is noteworthy that decay of unspliced pre-mRNA of NIPP1-RATA-transfected cells was slightly slower than that seen in mock-transfected cells (Fig. 2, *C* and *D*).

Taken together, these results demonstrate physical and functional association between NIPP1 and pre-mRNA splicing and suggest the importance of the NIPP1 C terminus and interaction between NIPP1 and PP1 in NIPP1-mediated regulation of splicing *in vivo*. When we performed an *in vitro* splicing assay in HeLa nuclear extracts, NIPP1-ΔC showed no effect as reported (Ref. 23 and data not shown). Based on these findings, we chose to evaluate NIPP1 function in cell-based rather than *in vitro* experiments.

Characterization of Splicing Inhibition by NIPP1-ΔC—To understand functional differences between NIPP1-ΔC and wild-type protein, we first investigated NIPP1-ΔC subcellular localization and found it indistinguishable from that of NIPP1-WT (Fig. 3*A*). We next prepared NIPP1 constructs containing point mutations in addition to the ΔC deletion to investigate domain requirements for splicing inhibition (Fig. 3*B*). The effects of these mutations on splicing of the β-globin construct were determined by analyzing accumulation of unspliced pre-mRNA. An RPA analysis revealed that NIPP1-ΔC, but not NIPP1-R53A/ΔC or NIPP1-RATA/ΔC, inhibited pre-mRNA splicing of the reporter gene (Fig. 3*C*). These results indicate that inhibition of splicing by NIPP1-ΔC requires both a functional FHA domain and interaction with PP1. Neither the R53A nor RATA mutation alone promoted accumulation of unspliced pre-mRNA (Fig. 1*B* and data not shown).

Because splicing inhibition by NIPP1-ΔC requires interaction with PP1, we compared NIPP1-WT and -ΔC mutant in terms of association with PP1. NIPP1-WT and NIPP1-ΔC were immunoprecipitated, and PP1 activities were evaluated using phosphorylase *a* as a substrate. PP1 activity complexed with NIPP1-ΔC was reproducibly higher than that seen with NIPP1-WT (Fig. 4*A*). Similar amounts of PP1 in immunoprecipitates of NIPP1-WT or -ΔC were confirmed by immunoblotting with anti-PP1 antibody (Fig. 4*B*). We reasoned that differences seen in Fig. 4*A* could be due to potential modification of the catalytic subunit PP1. It is well established that PP1 is phosphorylated by cyclin-dependent kinase(s) on a critical Thr residue in the C terminus (Thr-320 of PP1α) and inactivated (11, 12). NIPP1-WT or NIPP1-ΔC was immunoprecipitated from transfected cells, and the inhibitory phosphorylation of endogenous PP1 associated with NIPP1 was examined and compared. Strikingly, PP1 co-immunoprecipitated with NIPP1-WT was highly phosphorylated on the inhibitory site, whereas PP1 in association with NIPP-ΔC was minimally phosphorylated (Fig. 4*B*). Thus, the higher specific activity of PP1 associated with NIPP1-ΔC could be due to lower levels of inhibitory phosphorylation of PP1, rendering it constitutively active. At present, we cannot differentiate the levels of inhibitory phosphorylation in each PP1 isoforms because the phospho-Thr-320-PP1α antibody may also cross-react with other isoforms phosphorylated on the corresponding residue. Nevertheless, given that NIPP1 preferentially associates with PP1α (see below), it is likely that phospho-PP1 co-immunoprecipitating with NIPP1 is primarily PP1α.

NIPP1-associated PP1 Regulates Sap155 Phosphorylation—To further analyze NIPP1 actions in pre-mRNA splicing, stable cell lines conditionally expressing WT and mutant forms of NIPP1 (HeLa-TetOff (HTO)-NIPP1 clones) were developed. In these clones, FLAG-NIPP1 proteins were detected 8 h after removal of Dox, and levels were maximal at about 24 h (Fig. 5*A*). Previous studies had identified several potential effectors of NIPP1 and/or PP1 such as Cdc5L, Sap155, and U5-116k (6, 18, 19, 34). Levels of phosphorylation of these proteins in HTO-NIPP1 clones were investigated by metabolically labeling cells with ^{32}P-orthophosphate. We found that Sap155 hyperphosphorylation was slightly decreased in cells expressing WT-NIPP1 (Fig. 5*B*). Importantly, this decrease was more apparent in cells expressing NIPP1-ΔC. Induction of NIPP1-ΔC expression by Dox removal caused virtual loss of Sap155 hyperphosphorylation. The slight decrease in Sap155 hyperphosphorylation of HTO-NIPP1-ΔC cells in the presence of Dox was probably due to leaky expression of the construct in this system. In contrast, neither Cdc5L nor U5-116k phosphorylation levels were affected by NIPP1-WT or

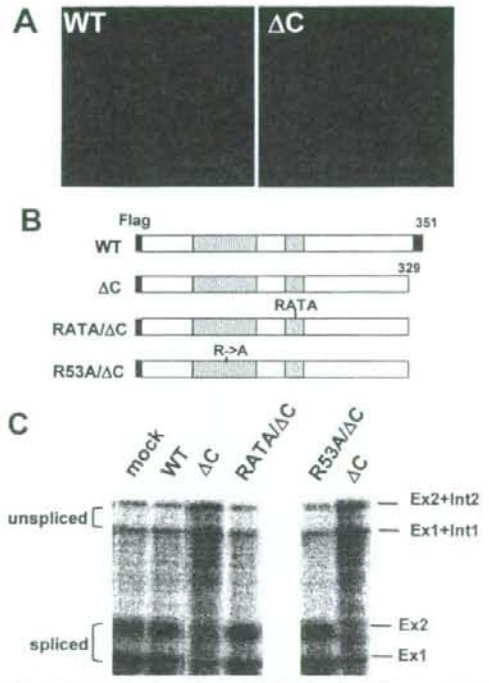

FIGURE 3. **Characterization of splicing inhibition by NIPP1-ΔC.** *A*, normal subcellular localization of NIPP1-ΔC. HTO cells were transiently transfected with NIPP1-WT or NIPP1-ΔC and subjected to immunostaining with the anti-FLAG antibody followed by Alexa Fluor488-conjugated anti-mouse IgG (*green*). F-Actin was co-stained with Alexa Fluor546-phalloidin (*red*). *B*, diagrams of NIPP1-ΔC and deleted forms further mutated in the FHA domain or the PP1-binding motif. *C*, HTO cells were transiently transfected with the β-globin reporter together with NIPP1 constructs shown in *B*. Total RNA was isolated and analyzed by RPA as in Fig. 2.

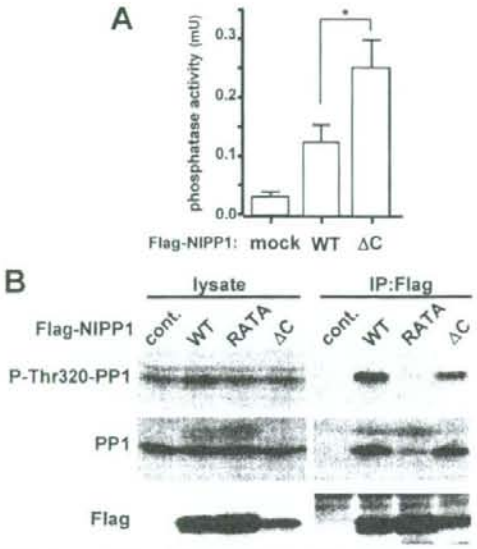

FIGURE 4. **Dysregulation of PP1 by NIPP1-ΔC.** *A*, PP1 activities in association with NIPP1-WT and -ΔC. HTO cells were transiently transfected with NIPP1-WT or NIPP1-ΔC and lysed, and immunoprecipitates with an anti-FLAG antibody were subjected to a phosphatase assay. Data represents mean of four independent experiments with S.D. *, $p < 0.05$. *B*, C-terminal inhibitory phosphorylation of PP1 associating with NIPP1-WT and NIPP1-ΔC. HTO cells were transiently transfected with NIPP1-WT or NIPP1-ΔC. After 24 h, cells were lysed and immunoprecipitated (*IP*) with an anti-FLAG antibody. Immunoblots were performed using anti-phospho-Thr-320-PP1α, anti-pan-PP1 (E9), or anti-FLAG antibodies. Anti-phospho-Thr-320-PP1α antibody also may cross-react with PP1γ and -δ isoforms phosphorylated on the corresponding residues (data from Cell Signaling Technology, Inc.). *Cont*, control.

-ΔC. Taken together, these results demonstrate that Sap155 is a major dephosphorylation target of PP1, which is regulated by NIPP1 *in vivo*.

To test the effects of NIPP1 depletion on Sap155 phosphorylation, parental HTO cells were transfected with NIPP1 siRNA to knockdown NIPP1 (Fig. 5*C*). Little effect of NIPP1 knockdown on Sap155 phosphorylation was observed, as judged by assaying Sap155 mobility shifts on Western blotting. We next treated NIPP1=knockdown cells with the cell-permeable toxin OA, which could preferentially inhibit PP2A class PPases (PP2A, PP4, and PP6) at the adopted concentration of 100 nM. OA treatment of mock- or control siRNA-transfected cells slightly increased levels of hyperphosphorylated Sap155 compared with vehicle-treated cells (Fig. 5*C*). In NIPP1-knockdown cells, OA-induced hyperphosphorylation of Sap155 was more robust than that seen in mock- or control siRNA-transfected cells (Fig. 5*C*). These results indicate the importance of endogenous NIPP1 in regulating Sap155 phosphorylation.

The results in Fig. 5, *B* and *C*, strongly suggest that NIPP1 promotes dephosphorylation of hyperphosphorylated Sap155 by associated PP1. We further tested this hypothesis by *in vitro* dephosphorylation experiments. As shown in Fig. 6*A*, OA treatment of cells greatly induced Thr phosphorylation of numerous cellular proteins (*lower panel*) and also hyperphosphorylation of Sap155 (*upper panel*). Incubation of cell lysates under dephosphorylation conditions (*i.e.* without PPase inhibitors) resulted in time-dependent loss of most phospho-Thr, likely because of the activities of endogenous PPase(s) other than PP1, but did not affect Sap155 phosphorylation. However, addition of recombinant PP1α led to complete loss of hyperphosphorylated Sap155 within 60 min, indicating that Sap155 is a PP1 substrate. Remarkably, further addition of NIPP1 enhanced dephosphorylation of hyperphosphorylated Sap155 (Fig. 6*B*). The stimulating effect of NIPP1 on Sap155 dephosphorylation by PP1 was also observed with immunopurified Sap155, minimizing the possibility that scaffolding proteins other than NIPP1 mediate this effect (Fig. 6*C* and supplemental Fig. 3*B*). Furthermore, Sap155/PP1 interaction was detectable by far-Western analysis only when PP1 was precomplexed with NIPP1 (Fig. 6*D*). Thus, we conclude that NIPP1 functions as a Sap155-targeting subunit for PP1.

Aberrant Sap155 Dephosphorylation Correlates with Inhibition of Pre-mRNA Splicing by Mutant NIPP1—How NIPP1 interacts with Sap155 was further investigated by immunoprecipitation assays. Sap155 was effectively co-immunoprecipitated with NIPP1-WT and -RATA but not with NIPP1-ΔC and -R53A (Fig. 7*A*). Importantly, Sap155 co-immunoprecipitated